NJC

Accepted Manuscript

This is an *Accepted Manuscript*, which has been through the Royal Society of Chemistry peer review process and has been accepted for publication.

Accepted Manuscripts are published online shortly after acceptance, before technical editing, formatting and proof reading. Using this free service, authors can make their results available to the community, in citable form, before we publish the edited article. We will replace this *Accepted Manuscript* with the edited and formatted *Advance Article* as soon as it is available.

You can find more information about *Accepted Manuscripts* in the Information for Authors.

Please note that technical editing may introduce minor changes to the text and/or graphics, which may alter content. The journal's standard Terms & Conditions and the Ethical guidelines still apply. In no event shall the Royal Society of Chemistry be held responsible for any errors or omissions in this *Accepted Manuscript* or any consequences arising from the use of any information it contains.

ROYAL SOCIETY OF CHEMISTRY

www.rsc.org/njc

New J. Chem.

RSCPublishing

ARTICLE

Heterometallic complexes† combining $[Mn^{III}(salpn)]^+$ and $[Fe(CN)_6]^{4-}$ units as the products of reactions between $[Mn^{III}(salpn)(H_2O)C(CN)_3]$ and $[Fe(CN)_6]^{3-/4-}$

Cite this: DOI: 10.1039/x0xx00000x

Received 00th March 2014,
Accepted 00th 2014

DOI: 10.1039/x0xx00000x

www.rsc.org/

Vyacheslav A. Kopotkov,[a*] Eduard B. Yagubskii,[a*] Sergey V. Simonov,[b] Leokadiya V. Zorina,[b*] Denis V. Starichenko,[c] Alexander V. Korolyov,[c] Vladimir V. Ustinov[c] and Yurii N. Shvachko[c,d*]

Reaction of $[Fe(III)(CN)_6]^{3-}$ with neutral $[Mn(salpn)(H_2O)C(CN)_3]$ (salpn: *N,N'*-propylenebis(salicylideneiminato)) (**1**) produces two new heterometallic complexes $[\{Mn^{III}(salpn)(H_2O)\}_2\{Mn^{III}(salpn)(H_2O)_{0.7}(CH_3OH)_{0.3}\}_2Fe^{II}(CN)_6]\cdot n(H_2O/CH_3OH)$ (**2**) and $[\{Mn^{III}(salpn)\}_4\{Mn^{III}(salpn)(H_2O)\}_2Fe^{II}(CN)_6]\{C(CN)_3\}_2\cdot 4H_2O$ (**3**), which are characterized by single-crystal X-ray diffraction. In this reaction, the $[C(CN)_3]^-$ ligand reduces Fe(III) to Fe(II). Complex **3** can be prepared directly using hexacyanoferrate(II). One more complex containing the hexacyanoferrate(II), $[\{Mn^{III}(salpn)(CH_3OH)_{0.67}(H_2O)_{0.33}\}_6Fe^{II}(CN)_6]\{ClO_4\}_2\cdot 8H_2O$ (**4**) is obtained in reaction of $[Fe(II)(CN)_6]^{4-}$ with cation complex $[Mn_2(salpn)_2(H_2O)_2](ClO_4)_2$. The iron(II) centers in the complexes **2** and **4** are linked via cyano-bridges with the four and six $[Mn^{III}(salpn)]^+$ fragments, respectively. The structure of **3** consists of the cyano-bridged $[Mn^{III}_6Fe^{II}]$ repeating units linked by double phenolate bridges into a one-dimensional polymeric chain. The magnetic properties of **3** indicate a ferromagnetic coupling between Mn^{III} centers in double-phenolate-bridged $[Mn^{III}(salpn)]_2$ dinuclear subunits. Quantum calculations within the Heisenberg−Van Vleck model are performed giving the exchange constant J = 0.64 cm^{-1} and zero-field splitting parameter D= −3.4±0.5 cm^{-1}. The ac-susceptibility obeys the Arrhenius law with the activation energy E_a=11.89 cm^{-1}.

Introduction

The manganese(III) ions form high-spin complexes with the tetradentate (N_2O_2) Schiff bases (SB) of salen type[1] (salen = *N,N'*-ethylenebis(salicylideneiminato) dianion; Scheme 1). Depending on steric features of the Schiff base, the nature of the terminal ligands, and the solvent, the complexes can exist in monomeric or the phenoxo-bridged dimeric forms (Scheme 2) with antiferromagnetic[2] or ferromagnetic[1f,3] intra-dimer interaction.

These complexes have been extensively used as building blocks for development of magnetic materials with variable dimensionality. The neutral terminal ligands were usually replaced by the paramagnetic bridging groups, in particular the hexacyanometalate anions ($[M(CN)_6]^{3-}$, M = Fe, Cr, Mn, Ru, Os).[3a,4]

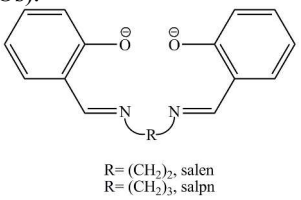

Scheme 1

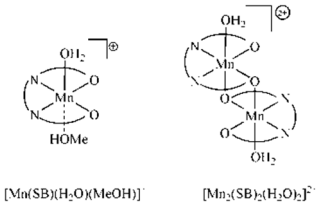

Scheme 2

Self-assemblies of $[Mn(SB)]^+$ and the hexacyanometalates bring forth the diverse structures (0D assemblies, 1D chains, 2D and 3D networks) showing the ferromagnetic superexchange coupling. In particular, the molecular nanomagnets such as single-molecule magnets (SMMs)[3e,g,4a,m,n] or single-chain magnets (SCMs)[4e,5] exhibiting a slow relaxation of magnetization have been found among them.

Recently, we have synthesized a series of neutral Mn(III) salen type Schiff base complexes containing tricyanometanide-ion $[C(CN)_3]^-$ as terminal ligand.[6] In this paper, the reactions with one of these complexes, namely, $[Mn(salpn)(H_2O)C(CN)_3]$ (**1**), where salpn = *N,N'*-1,3-propylenebis(salicylideneiminato) dianion, with hexacyanoferrate(III) and hexacyanoferrate(II) have been studied. As a result, the complexes containing the hexacyanoferrate(II), $[\{Mn(salpn)(H_2O)\}_2\{Mn(salpn)(H_2O)_{0.7}(CH_3OH)_{0.3}\}_2Fe(CN)_6]\cdot n(H_2O/CH_3OH)$ (**2**) and $[\{Mn(salpn)\}_4\{Mn(salpn)(H_2O)\}_2Fe(CN)_6]\{C(CN)_3\}_2\cdot 4H_2O$ (**3**), have been synthesized. For comparison we also studied the reaction of the cation complex $[Mn_2(salpn)_2(H_2O)_2](ClO_4)_2$ with the hexacyanoferrate(II) and have obtained one more $[Fe^{II}(CN)_6]^{4-}$-bridged complex, $[\{Mn(salpn)(CH_3OH)_{0.67}(H_2O)_{0.33}\}_6Fe(CN)_6]\{ClO_4\}_2\cdot 8H_2O$ (**4**). The crystal structures of **2**, **3**, **4** as well as the magnetic properties of **3** are studied in current work.

Results and discussion

Synthesis

The addition of $[Mn(salpn)(H_2O)C(CN)_3]$ in CH_3OH to solution of $K_3[Fe(CN)_6]$ in H_2O gives rise to the formation of crystals in the process of slow evaporation of mother liquor for one week or so. An X-ray diffraction of several separated crystals shows the availability of three different phases. The compositions of two of them was determined from full X-ray analysis: $[\{Mn(salpn)(H_2O)\}_2\{Mn(salpn)(H_2O)_{0.7}(CH_3OH)_{0.3}\}_2Fe(CN)_6]\cdot n(H_2O/CH_3OH)$ (**2**) and $[\{Mn(salpn)\}_4\{Mn(salpn)(H_2O)\}_2\{Fe(CN)_6\}]\{C(CN)_3\}_2\cdot 4H_2O$ (**3**) (Scheme 3). The attempts to prepare the single-phase samples by the variation of molar ratio of starting reagents have failed. The analysis of charge balance in the compounds **2**, **3** points to the presence of Fe(II) rather than Fe(III) ions. Earlier the reduction of the ferricyanide to ferrocyanide was observed in the reactions of Cu^{II}, Ni^{II} and Mn^{II} complexes with $[Fe(III)(CN)_6]^{3-}$.[7] The reason for this reduction remains unclear. In our case the tricyanometanide ligand is likely to reduce iron(III) to iron(II). To verify this deduction, we have studied the reaction of **1** with ferrocyanide $(NH_4)_4[Fe(CN)_6]$ and the reactions of the cation complex $[Mn_2(salpn)_2(H_2O)_2](ClO_4)_2$ with ferri- and ferrocyanides. In the first reaction, the complex **3** is obtained as single-phase product at the molar ratios of 4:1 and 6:1 of the starting reagents. This was confirmed by the data of single crystal and powder X-ray diffraction and elemental analysis. The IR spectrum of **3** showed the band at 2050 cm^{-1}, which corresponds to the stretching mode of the bridging CN groups attached to Fe^{II}.[7] In two other reactions, one more $[Fe^{II}(CN)_6]^{4-}$-bridged complex, $[\{Mn(salpn)(CH_3OH)_{0.67}(H_2O)_{0.33}\}_6Fe(CN)_6]\{ClO_4\}_2\cdot 8H_2O$ (**4**) is obtained in the reaction with ammonium ferrocyanide, whereas the known complex $[\{Mn^{III}(salpn)(CH_3OH)\}_4Fe^{III}(CN)_6]ClO_4\cdot 9H_2O$[8] appears in the reaction with potassium ferricyanide (Scheme 4). The formation of complexes containing Fe(II) ions in the reactions of $[Mn^{III}(SB)]$ with $[Fe^{II}(CN)_6]^{4-}$ testifies that the redox reaction between Mn^{III} and Fe(II) ions does not happen unlike the redox behavior of $[Mn^{III}(SB)]^+$ – $[W^{IV}(CN)_8]^{4-}$ system in which $[W^V(CN)_8]^{3-}$ anions are formed.[9]

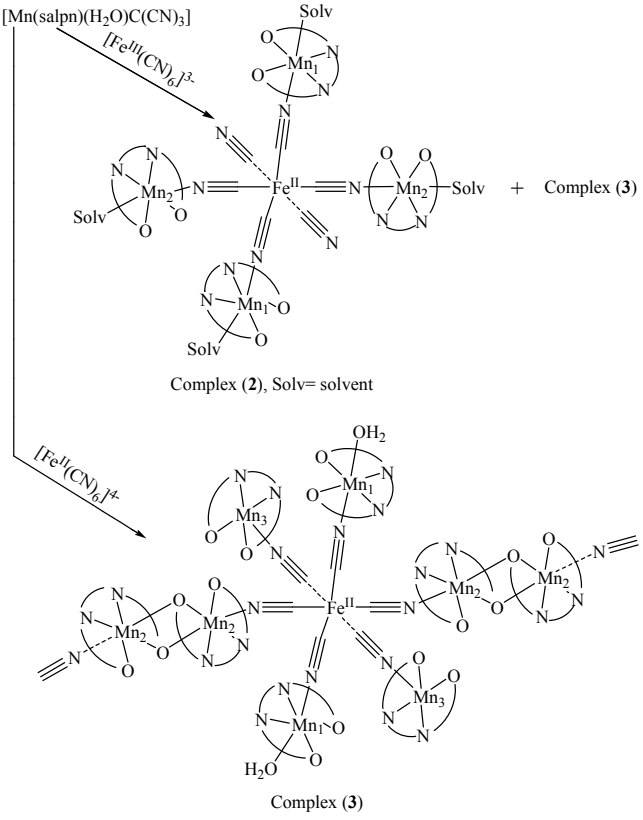

Scheme 3

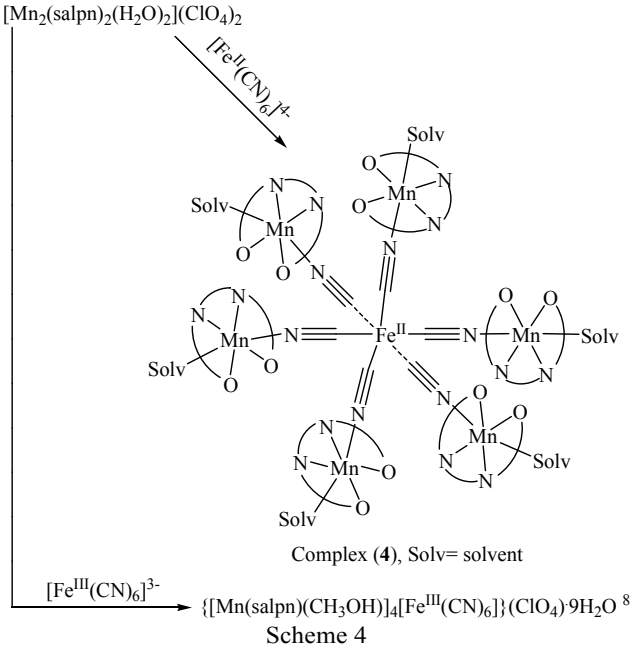

Scheme 4

Crystal structures

$[\{Mn(salpn)(H_2O)\}_2\{Mn(salpn)(H_2O)_{0.7}(CH_3OH)_{0.3}\}_2Fe(CN)_6]\cdot n(H_2O/CH_3OH)$ (2). Complex **2** crystallizes in the

monoclinic $P2_1/c$ space group. The asymmetric unit includes 1/2 of a neutral pentanuclear complex with inversion symmetry on its central Fe^{II} ion. An ORTEP drawing of **2** is shown in Fig. 1, key bond distances and angles are listed in Table 1. Four equatorial CN-ligands of the $[Fe^{II}(CN)_6]^{4-}$ octahedron coordinate axially to Mn from four $[Mn(salpn)]^+$ moieties. Fe–C bond lengths vary from 1.930(3) to 1.940(3) Å. All the Mn^{III} centers are hexacoordinated, with two N and two O atoms of the salpn ligand in the equatorial plane while two axial positions are occupied by the N atom from the bridging cyanide ligand and the oxygen atom of terminal H_2O or CH_3OH ligand. In the axial direction, the $Mn–O_{aqua/methanol}$ and $Mn–N_{cyanide}$ bond distances are elongated in comparison with the equatorial bonds due to a Jahn–Teller (JT) distortion at the 3d metal center (see Table 1). There are two independent Mn^{III} ions in the complex. Salpn unit at Mn1 has nearly flattened geometry (Fig. 1) and its aqua ligand
forms hydrogen bonds within the *bc* layer (Figure S1) with the phenolate oxygen of neighboring inversionally related Mn1 unit and non-bridging nitrogen atom of the $Fe(CN)_6$ core of another neighbor. Second [Mn(salpn)] unit is strongly bent and these units from adjacent *bc* layers are nested with each other without hydrogen bonding (Figure S2). Free space between the complexes is filled by strongly disordered water and methanol molecules.

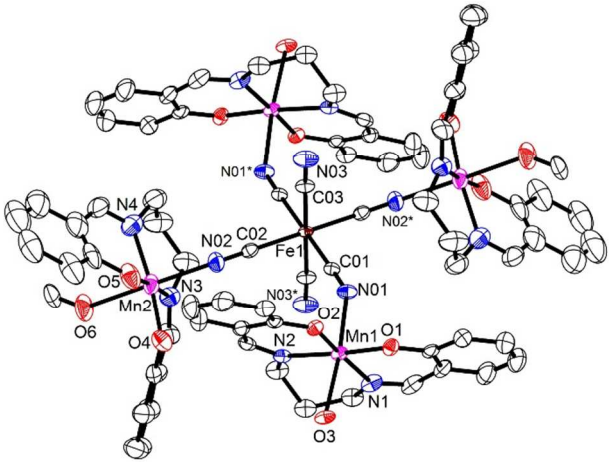

Fig. 1. ORTEP drawing of a pentanuclear unit in **2** with 50% probability ellipsoids and partial atom numbering scheme (only major part of disordered groups is shown). Fe1 is at an inversion centre, symmetry code:* (-*x*, 1-*y*, -*z*).

The $[Mn^{III}_4Fe^{II}]$ units in **2** are discrete. Previously the similar pentanuclear units were found in the cationic complex $[\{Mn^{III}(salpn)CH_3OH\}_4Fe^{III}(CN)_6]^+$ (**5**), containing ferricyanide fragment.[8] Although **2** and **5** have similar molecular structures, their crystal packings differ essentially. Furthermore, two polymeric structures containing $[Mn^{III}_4Fe^{II}]$ motifs connected into 2D networks through biphenolate Mn(saltmen)–(μ-$O)_2$–Mn(saltmen) bridges or common $[Mn^{III}(salen)]^+$ fragments were synthesized with the $[Fe^{II}(CN)_5NO]^{2-}$ building block.[10]

Table 1. Selected bond lengths (Å) and angles (º) in **2**

Mn(1)-N(1)	2.041(3)	Mn(2)-N(3)	2.045(5)
Mn(1)-N(2)	2.040(3)	Mn(2)-N(4)	2.019(6)
Mn(1)-O(1)	1.898(3)	Mn(2)-O(4)	1.882(5)
Mn(1)-O(2)	1.876(2)	Mn(2)-O(5)	1.886(5)
Mn(1)-N(01)	2.279(3)	Mn(2)-N(02)	2.179(5)
Mn(1)-O(3)	2.241(2)	Mn(2)-O(6)	2.337(6)
N(01)-Mn(1)-O(3)	172.2(1)	N(02)-Mn(2)-O(6)	171.6(2)
Mn(1)-N(01)-C(01)	145.4(3)	Mn(2)-N(02)-C(02)	160.1(3)
N(01)-C(01)-Fe(1)	178.7(3)	N(02)-C(02)-Fe(1)	175.6(3)

[{Mn(salpn)}$_4${Mn(salpn)(H$_2$O)}$_2$Fe(CN)$_6$]{C(CN)$_3$}$_2$·4H$_2$O (3). Complex **3** crystallizes in the monoclinic $P2_1/n$ space group. The asymmetric unit contains 1/2 of a heptanuclear dicationic complex with the Fe^{II} ion at an inversion center, one $\{C(CN)_3\}^-$ anion and two water molecules in general positions. An ORTEP drawing of unique atoms of complex **3** is shown in Fig. 2, key bond distances and angles are listed in Table 2. All six CN-ligands of the $[Fe^{II}(CN)_6]^{4-}$ octahedron are bridged axially to Mn from six surrounding $[Mn(salpn)]^+$ moieties. Fe–C bond lengths vary from 1.904(3) to 1.918(3) Å.

There are three independent Mn^{III} ions in the complex. The cyanide bridge and the aqua ligand at Mn(1) ion are arranged in the *trans* position leading to a local distorted octahedral coordination geometry of Mn(1). The Jahn–Teller distortion leads to elongated axial $Mn–N_{cyanide}$ and $Mn–O_{aqua}$ bonds in the Mn(1) octahedron of 2.183(3) and 2.300(2) Å, respectively.

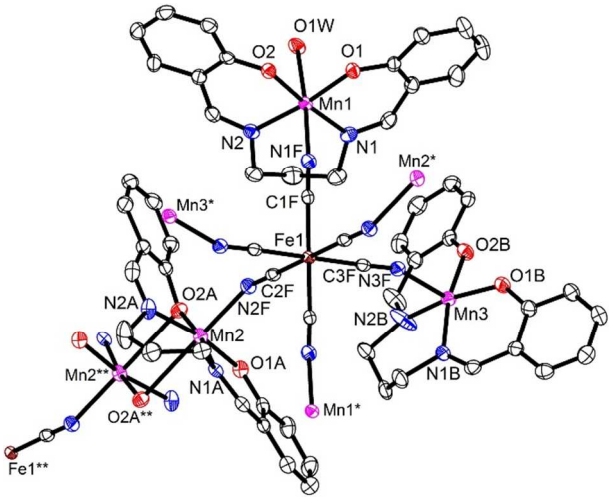

Fig. 2. ORTEP drawing of unique atoms of a heptanuclear unit in **3** with 50% probability ellipsoids and partial atom numbering scheme. Fe1 is at an inversion centre, symmetry codes: * (1-*x*, 1-*y*, -*z*), ** (-*x*, 1-*y*, -*z*)

The Mn(2) ions form double phenolate bridges $[\{Mn(NC)(salpn)\}(\mu–O_{phenolate})_2\{Mn(NC)(salpn)\}]$ between the neighboring $[Mn^{III}_6Fe^{II}]$ units (Fig. 2) linking them into one-dimensional polymeric chain along the *a* direction (Fig. 3).

Within the connecting $(Mn^{III})_2$ dimers, Mn(2) centers are surrounded by two N and two O atoms of the salpn ligand in the equatorial plane, one axial N atom from the cyanide bridge and one axial O atom from the neighboring $[Mn^{III}(salpn)]^+$ moiety. The Jahn–Teller elongation axis in the Mn(2) octahedron lies along the axial direction with $Mn–N_{cyanide}$ and $Mn–O_{phenolate}$ bonds of 2.167(3) and 2.697(2) Å. The $Mn^{III}–Mn^{III}$ distance in the dimeric moiety is 3.491(1) Å, while the Mn–O–Mn and

Table 2. Selected bond lengths (Å) and angles (º) in **3**

Mn(1)-N(1)	2.043(3)	Mn(2)-N(1A)	1.994(3)
Mn(1)-N(2)	2.029(3)	Mn(2)-N(2A)	2.024(3)
Mn(1)-O(1)	1.883(2)	Mn(2)-O(1A)	1.891(2)
Mn(1)-O(2)	1.900(2)	Mn(2)-O(2A)	1.900(2)
Mn(1)-N(1F)	2.183(3)	Mn(2)-N(2F)	2.167(3)
Mn(1)-O(1W)	2.300(2)	Mn(2)-O(2A**)	2.697(2)
N(1F)-Mn(1)-O(1W)	174.2(1)	N(2F)-Mn(2)-O(2A**)	178.4(1)
Mn(1)-N(1F)-C(1F)	162.2(3)	Mn(2)-N(2F)-C(2F)	144.6(3)
N(1F)-C(1F)-Fe(1)	177.5(3)	N(2F)-C(2F)-Fe(1)	173.9(3)
		Mn(2) – O(2A)-Mn(2**)	97.32(9)
Mn(3)-N(1B)	2.030(3)		
Mn(3)-N(2B)	2.031(3)	Mn(3)-N(3F)-C(3F)	157.9(3)
Mn(3)-O(1B)	1.893(2)	N(3F)-C(3F)-Fe(1)	175.8(3)
Mn(3)-O(2B)	1.873(2)		
Mn(3)-N(3F)	2.078(3)		

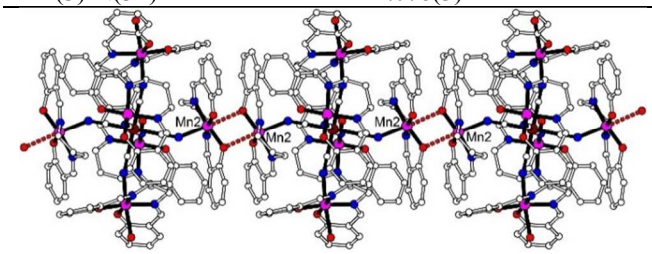

Fig. 3. A fragment of 1D polymeric chain running along the *a*-axis in the structure **3**. Mn(2)-μ-O bridges between the $[Mn_6Fe]^{2+}$ units are shown by red dashed lines.

O−Mn−O angles are 97.32(9)º and 82.68º, respectively. The Fe^{II}–Mn^{III} intramolecular distances in the complex **3** are shorter along the direction of the infinite dimeric chains (4.969(2), 5.066(1) and 5.188(1) Å for Mn(2), Mn(3) and Mn(1), respectively) due to smaller Mn(2)−N≡C angle (Table 2).

The Mn(3) ion has a distorted square pyramidal coordination geometry in which apical site is occupied by the nitrogen atom of the bridging CN group. Mn(3) moieties are hydrogen bonded to Mn(1) moieties through oxygen atoms of phenolate and aqua ligand along two directions, [111] and [$1\bar{1}$ 1], to generate a 2D layer framework parallel to the ($10\bar{1}$) plane (Figure S3); the Mn(1)−Mn(3) distance in this contact is 5.695(1) Å. The $\{C(CN)_3\}^-$ anions are linked by N_{anion}…H−O−H…N_{anion} bonding through one of the free water molecules into infinite chains along the *b*-axis and additionally to the aqua ligand of the complex through the same water molecule. Another water molecule forms a bridge between the anion and the phenolate oxygen atom of the Mn(2) moiety. Some heptanuclear complexes $[Fe^{III}(CN)_6\{Mn^{III}(SB)\}_6]$ (SB= salen and its derivatives) with similar coordination but different valent state of the central Fe ion (paramagnetic Fe^{III} instead of diamagnetic Fe^{II} in **3**) were reported earlier. In most of these compounds the heptanuclear complexes are discrete[11] and only in one compound two types of chain motifs are found.[4i] In one direction, the heptanuclear complexes are linked by biphenolate bridges, as in **3**, while in perpendicular direction they are connected through additional $[Fe(CN)_6]^{3-}$ units resulting in infinite chain of alternating cyano-bridged Fe^{III} and Mn^{III} ions: $-[N{\equiv}C\text{-}Fe^{III}\text{-}C{\equiv}N]_{anion}-[Mn^{III}\text{-}N{\equiv}C\text{-}Fe^{III}\text{-}C{\equiv}N\text{-}Mn^{III}]_{complex}-$.
The sole known heptanuclear complex with Fe^{II} central ion, $[Fe^{II}(CN)_6\{Mn^{III}(salen)\}_6]$, is integrated into a 3D structure in which all $[Fe^{II}Mn^{III}_6]$ units are interconnected through diamagnetic $[Nb_6Cl_{12}(CN)_6]^{4-}$ building blocks.[12] Other examples of infinite chains through phenolate bridges are found in complexes with Mn^{III}(SB) moieties connected to $[Cr^{III}(CN)_6]^{3-}$, $[Mo(CN)_8]^{4-}$ or $[Nb_6Cl_{12}(CN)_6]^{4-}$.[9,13,14]

$[\{Mn(salpn)(CH_3OH)_{0.67}(H_2O)_{0.33}\}_6Fe(CN)_6]\{ClO_4\}_2\cdot 8H_2O$ (4). Complex **4** crystallizes in the cubic $Pa\bar{3}$ space group. The asymmetric unit contains 1/6 of a heptanuclear cationic complex with the Fe^{II} ion at $\bar{3}$ position, 1/3 of $\{ClO_4\}^-$ anion at a three-fold axis and two water molecules in general positions one of which is 0.33 occupied. An ORTEP drawing of unique atoms of complex **4** is shown in Fig. 4, key bond distances and angles are listed in Table 3.

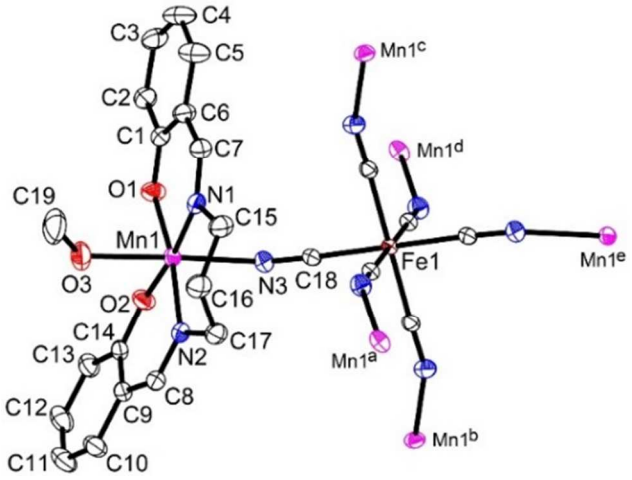

Fig. 4. ORTEP drawing of unique atoms of a heptanuclear unit in **4** with 50% probability ellipsoids and atom numbering scheme. Fe1 is at $\bar{3}$ position, symmetry codes: a (1-z, x-0.5, 0.5-y), b (y+0.5, 0.5-z, 1-x), c (0.5-y, z-0.5, x), d (z, 0.5-x, y +0.5), e (1-x, -y, 1-z).

All six CN-ligands of the $[Fe^{II}(CN)_6]^{4-}$ octahedron (Fe−C = 1.904(1) Å) are bridged axially to Mn from six surrounding $[Mn(salpn)]^+$ moieties. The sole independent Mn^{III} ion has distorted octahedral coordination geometry, the trans position to the cyano bridge is occupied with methanol or aqua ligand in 0.67/0.33 ratio. Axial Mn−$N_{cyanido}$ and Mn−$O_{methanol/aqua}$ bonds of 2.168(1) and 2.294(1) Å, respectively, are elongated due to

the Jahn–Teller distortion. The $[Mn_6Fe]^{2+}$ complexes in **4** are isolated and interact only with anions [(C)H_{salpn}…O_{anion} 2.44 Å] and free water molecules (O–$H_{methanol/aqua}$…O_{water} 1.85 Å, O–H_{water}…O_{salpn} 2.03 and 2.44 Å).

Table 3. Selected bond lengths (Å) and angles (º) in **4**

Mn(1)-N(1)	2.045(1)
Mn(1)-N(2)	2.036(1)
Mn(1)-O(1)	1.900(1)
Mn(1)-O(2)	1.896(1)
Mn(1)-N(3)	2.168(1)
Mn(1)-O(3)	2.294(1)
N(3)-Mn(1)-O(3)	168.16(6)
Mn(1)-N(3)-C(18)	148.2(1)
N(3)-C(18)-Fe(1)	177.6(1)

Magnetic properties of complex 3

Temperature dependences of the magnetic susceptibility, χ(T), T=2−300 K were measured on a polycrystalline sample of **3** in the external magnetic fields H=4 kOe and 40 kOe. The product χT is depicted on Fig. 5. The room-temperature χT value of 17.0 cm^3 K mol^{-1} (11.7 μ_B) is in good agreement with the paramagnetic response of the six Mn^{III} cations with S=2, and g=1.94. Hence, the Fe^{II} cation does not contribute to the magnetic susceptibility, *i.e.* it has low spin electronic configuration with S=0. The χT curve measured in cooling regime at the field 4 kOe remains nearly temperature independent in the range 300−24 K, then slightly (~2%) increases reaching maximum of 18.4 cm^3 K mol^{-1} (12.1 μ_B) at 5.9 K, and returns to 14.4 cm^3 K mol^{-1} at 2.0 K. The χT curve measured in the high field of 40 kOe while heating demonstrates a pronounced depression in the range 2−15 K starting from 16.6 cm^3 K mol^{-1} at 15 K and reaching 4.5 cm^3 K mol^{-1} (6.0 μ_B) at 2.0 K. In the interval 15−300 K the χT value remains nearly temperature independent within the range 17.1−16.4 cm^3 K mol^{-1}. Temperature behavior of the reciprocal magnetic susceptibility χ^{-1}(T) is shown on the inset. Fitting the data with the Curie-Weiss law (solid line) gives the Curie constant of 16.8 cm^3 K mol^{-1} (4 kOe) and the Weiss constant of θ=+1.2 K (R-factor=0.9999), indicating a presence of weak ferromagnetic interactions. The low temperature descent of the χT points at 40 kOe correlates with the field dependence and has different nature.

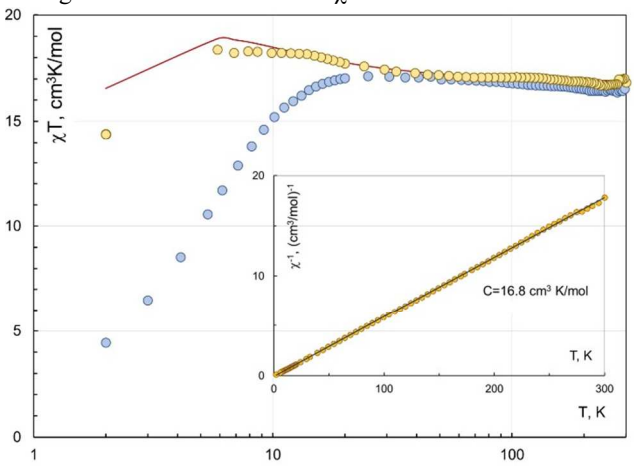

Fig. 5. Temperature dependence of the product χT for a polycrystalline sample of **3** in the fields of 4 kOe and 40 kOe. Solid red line is the best fit approximation using Heisenberg-Van Vleck model for the Mn(III) dimers with the parameters H=4 kOe, g=1.94, $J_{2,2}$=0.64 cm^{-1}, D_{PM}=-0.5 cm^{-1}, D_D=-3.0 cm^{-1} (see text).

The inset is temperature dependence of the reciprocal magnetic susceptibility χ^{-1} measured at 4 kOe. Solid line on the inset is the Curie-Weiss approximation with the Curie constant C= 16.8 cm^3K/mol and Weiss temperature Θ=1.2 K

The isothermal magnetization curve M(H/T), T=2.0 K is shown in Fig. 6. In the plot the applied magnetic field was slowly reversed from +50 to −50 and back to +50 kOe. The experimental points at the same fields coincide. The magnetization value at 50 kOe is 17.1 μ_B, which is approximately 2/3 of the theoretical value of 24 μ_B for 6 independent moments S=2 in the complex **3**. The Brillouin curves for six and four paramagnetic spin moments S=2 are depicted as blue and red solid lines respectively. The inset shows in a greater scale the interval −2.5 to +2.5 kOe.

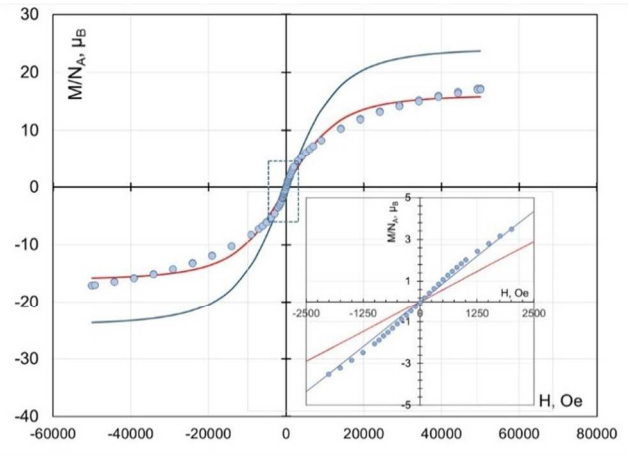

Fig. 6. Field dependences of the magnetization M(H) measured at T=2.0 K for a polycrystalline sample **3**. Solid lines are Brillouin approximations for six (blue line) and four (red line) paramagnetic moments S=2

The magnetic behavior in smaller magnetic fields, H< 2.5 kOe is qualitatively different compare to that in higher fields. While in low fields all six Mn^{III} spin moments contribute to the magnetization, in higher fields the experimental points appears to follow the Brillouin curve for 4 Mn^{III} moments. Such "S"-type curvature looks opposite to that observed for superparamagnetic systems. This unusual field dependence may indicate strong anisotropy for specific pair of Mn^{III} moments.

The structure of **3** contains 1D chains. They are stabilized by π-stacking of the lateral salpn ligands co-ordinating Mn(2) and Mn(2**) ions on adjacent [{Mn(salpn)}$_4${Mn(salpn)(H_2O)}$_2$Fe$(CN)_6$] units (Fig. 3, 7). The distance Mn(2)−Mn(2**), d=3.491(1) Å, is short enough to assume magnetic coupling in the Mn^{III} dimer. The Mn(2) and Mn(2**) positions are located within the elongated octahedra with antiparallel long axes [N(2F), O(2A**)] and [N(2F**), O(2A)] (see Fig. 7C).

The position of Mn(2)/Mn(2**) is strongly displaced on the axis from the center towards N(2F)/N(2F**) of the CN-ligand (difference between Mn(2)−N(2F) and Mn(2)−O(2A**) distances is 0.53 Å or 24% of the first bond distance, see Table 2). In this sense, these axes are "antiparallel". The distance [Mn(2), N(2F)]= 2.167 Å is close to the equatorial one [Mn(2),

N(2A)]= 2.024 Å with the difference of 0.14 Å or 6.5%. These specific distortions are lowering the symmetry and may induce mixing between the low-lying *d*-states. The oxygen O(2A**)/O(2A) remains considerably remote, 2.697 Å, because the C(12A) atom belongs to the rigid [C(12A), O(2A), Mn(2)] covalent claw. The claw is fixated by the π-stacking (see Fig. 7B). Thus, the π-stacking of the peripheral aromatic groups plays important role by inducing specific distortions in the co-ordination octahedra. In turn they may strongly affect the energy spectrum of *d*-orbitals and single ion magnetic anisotropy, causing unusual field dependence of the magnetization.

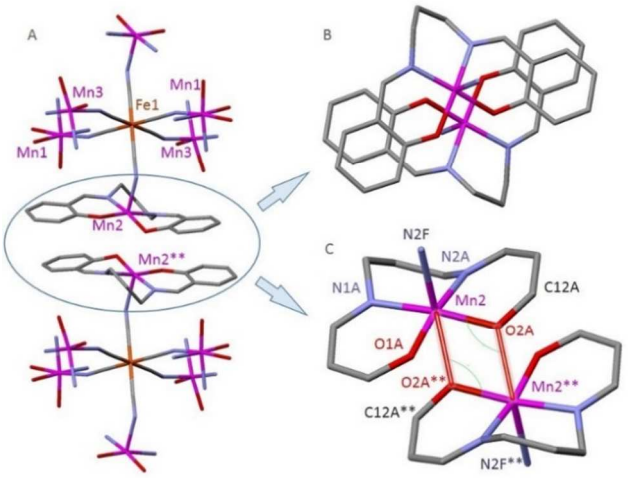

Fig. 7. Schematic view of the Mn(III) dimer in complex **3** showing the co-ordination sites:

A. co-ordination sites of 3d cations Mn(III) and Fe(II);

B. π–stacking of salpn ligands;

C isolated dimer Mn(2)-Mn(2**) on adjacent $[Mn^{III}_6Fe^{II}]$ units.

In the following analysis of the low-field curve χ(T) the low-symmetry distortions were not taken into consideration. The elongation ratio, *i.e.* the ratio of the distances [N(2F), O(2A**)] to [O(1A), N(2A)] (see Fig. 7C), is 1.25. Formally, this allows considering the Jahn−Teller energy diagram $t_{2g}^3e_g^1$ for the Mn^{III} *d*-levels at Mn(2) sites.[1f] Note, that the elongated axes ([N(2F), O(2A**)], [N(2F**), O(2A)]) lay in the "super-exchange plane", [Mn(2), O(2A), Mn(2**)].

In the numerical simulations, we considered two additive contributions to the total magnetic susceptibility χ_T:

$$\chi_T = (4+2\alpha)\cdot\chi_\rho + (1-\alpha)\cdot\chi_{dimer} \quad (1)$$

where χ_p and χ_{dimer} are paramagnetic susceptibilities of individual non-interacting spin moment S=2, and exchange coupled pair respectively; $(4+2\alpha)$ and $(1-\alpha)$ are weight coefficients. In the ideal case of infinite chain, $\alpha = 0$. Due to defects in real structure, some dimers can be broken. Respectively, the weight coefficients would vary resulting in $\alpha > 0$. In the "no coupling" case, $\alpha = 1$, *i.e.* six non-interacting Mn^{III} moments are observed.

For paramagnetic contribution, χ_ρ, we took the Curie–Weiss dependence, with the fixed parameters S=2, *g*=1.94, and variable *D* constant. For simulation of the dimer contribution we used the Heisenberg–Van Vleck model and the following spin Hamiltonian:

$$H = H_{ex} + H_{ZFS} + H_Z \quad (2),$$

where

$$H_{ex} = -2\cdot J_{22'}\cdot\overrightarrow{S_2}\overrightarrow{S_{2'}} \quad (3)$$

is the Heisenberg exchange Hamiltonian,

$$H_{ZFS} = D_2\left[S^2_{Z,2} - \frac{1}{3}S_2(S_2+1)\right] + D_{2'}\left[S^2_{Z,2'} - \frac{1}{3}S_{2'}(S_{2'}+1)\right] \quad (4)$$

takes into account zero-field splitting (ZFS),

$$H_Z = g\cdot\beta\cdot\left(\overrightarrow{S_2} + \overrightarrow{S_{2'}}\right)\cdot\vec{B} \quad (5)$$

is the Zeeman interactions.

The intra-dimer exchange coupling between Mn^{III} moments in Mn2 and Mn2** positions was characterized by the parameter $J_{22'}$. Due to symmetry, the axial ZFS constants D_2, $D_{2'}$ were taken as a single parameter $D = D_2 = D_{2'}$, as well as the g-factors g_2, $g_{2'}$, $g_2 = g_{2'} = g$. Rhombic ZFS constants E_i were not taken into fiting, suggesting $E/D << 1$. Simulations of the experimental data were performed by using the julX program involving full diagonalization of the spin Hamiltonian.[15]

The weight coefficients and g-value were determined at 300 K. The balance between the experiment and the model was reached at g=1.94 giving $\alpha \approx 0$ – infinite alternating chains.

In general, the *D*-parameters have to be assigned to all Mn^{III} cations in the complex, including those at Mn(1), Mn(1**), Mn(3), Mn(3**) positions. However, they have distorted square pyramidal Mn(3), Mn(3**), and distorted octahedral Mn(1), Mn(1**) co-ordinations. Therefore, their ZFS parameters, D_{PM}, have to be smaller (or negligible) compare to *D* values of the Jahn-Teller cations in the dimer. We built a series of χ_p(T) curves for D=0 to -2.0 cm^{-1} and substracted them from the experimental data. Thus, we extracted the dimer contributions $\chi_{dimer} = \chi - 4\chi_\rho(D_{PM})$ for fitting, where D_{PM} determined a confidence interval. The fitting procedure is described in the supplementary materials.

The best-fit curve is shown in Fig. 5 as solid line with the parameters $J_{22'}$ =0.64 cm^{-1} and D=−3.5±0.5 cm^{-1}. The result of simulations is in good agreement with the experimental data down to 5 K for D_{PM} values from 0 to -0.5 cm^{-1}. The value of the parameter *D* is close to that published for the dimeric complex $[Mn_2(salpn)_2(H_2O)_2](ClO_4)_2$, D= −3.1 cm^{-1},[3f] and several other similar complexes.[1f, 3e,g] We have also found, that the best-fit curve for the high field (40 kOe) data is less sensitive to the *D* value, whereas for the low field (4 kOe) data the deviation of ΔD=0.2 cm^{-1} is essential for the agreement. Ferromagnetic intra-dimer coupling was also reported for a series of dimeric Mn^{III} compounds with saltmen^{2-} and naphtmen^{2-} ligands.[1f, 3e,g,f].

A positive sign of the coupling constant is qualitatively associated with superexchange between the orthogonal $(d_{z^2})^1$ and the d_π orbitals ($(d_{yz})^1$, $(d_{xz})^1$ and $(d_{xy})^1$ orbitals) via *p*-orbitals of the co-ordinating oxygen atom O* corresponding to O(2A)/O(2A**) in **3**. The empiric correlation between the Mn−O* distance and the magnetic exchange parameter J_F was evaluated for the bond range of 2.4–3.7 Å.[1f] Applying this evaluation to the dimer in the structure **3** one can obtain an estimate of –0.96 cm^{-1}, which is approximately 4 times smaller lower than the calculated $J_{22'}$ value. The later work[3g] also

reports the tetradentate Schiff base complex of similar type, within which the two Mn^{III} ions interact antiferromagntically despite of relatively short Mn−O* distance.

The alternating current (*ac*) magnetic susceptibility of **3** in the form of the out-of-phase component of the *ac* magnetic susceptibility, χ'', versus frequency *f* (Hz) plots was investigated in the temperature range 1.8 – 3.0 K. In zero *dc* magnetic field, χ'' curves demonstrate maximum that moves from the highest frequency *f*=10 kHz at 2.25 K down to 190 Hz at 1.80 K as shown in Fig. 8. The values of the relaxation time, which are calculated from the maximum of χ'' at a given frequency *f*, follow the Arrhenius law characteristic of a thermally activated mechanism ($\tau = \tau_0 exp(E_a/k_BT)$), k_B-Boltzman constant); solid line in the Fig. 9. The calculated values of the pre-exponential factor and the activation energy $\tau_0=6.9\cdot10^{-4}$ s and E_a=11.89 cm^{-1} (17.1 K) are consistent with those previously reported for Jahn-Teller ions Mn^{III}.[3g] The E_a value obtained for **3** compares reasonably well with the *D* estimate from the numeric simulations of the *dc* susceptibility data when we take S=2 ($E_a=DS^2=4D$=14 cm^{-1}). For S=4 the estimate of *D* from *ac*-measurements gives -0.74 cm^{-1}. This is because the measurements were performed at the temperatures much higher compare to the value of intra-dimer coupling constant ($J_{22'}=0.92$ K<< *2* K).

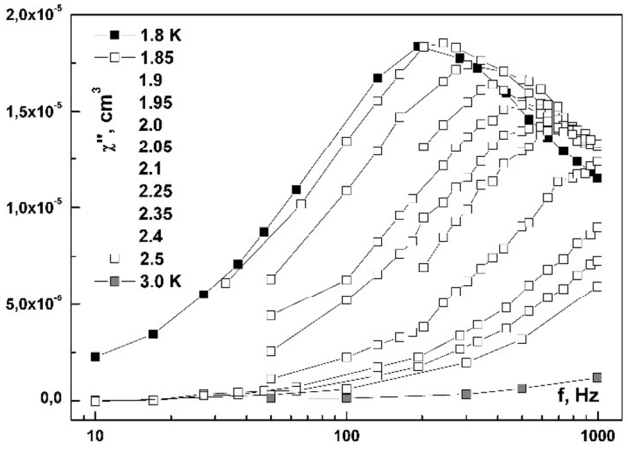

Fig. 8. Plot of the out-of-phase *ac* magnetic susceptibility, χ'', vs. frequency, *f*, for a polycrystalline sample **3** at the temperatures 1.8 K < T < 3.0 K and a 4.0 *G* oscillating field.

Although a ferromagnetic coupling in the compound **3** is in agreement similar dimeric compounds, its nature remains unclear. According to the Goodenough-Kanamori-Anderson rules[16a, b] a superexchange between single occupied $t_{2g}^3e_g^1$ *d*-orbitals is expected to be antiferromagnetic. Ferromagnetic coupling arises when virtual electron hopping is allowed from *p*-orbitals of O(2A) to one empty *d*-orbital of Mn(2) and one of the single occupied *d*-orbitals of Mn(2**) or vice versa. The oxygen O(2A) has three sp^2 orbitals, two of which are involved in covalent σ bonding with Mn(2) and C(12A). Their energies are located well below (approx. 5 eV) Fermi level ε_F, so they do not contribute to superexchange. There is only one double occupied *p*-orbital available. It is orthogonal to the plane [Mn(2), O(2A), C(12A)], which is formed by the sp^2 orbitals. We believe that the key factors influencing both sign and magnitude of the magnetic coupling are in-plane configuration of the JT axes and orientation of the *p*-orbital of the O(2A) oxygen relatively to the [Mn(2), O(2A), Mn(2**)] plane. In the compound **3** this orbital is not collinear to the octahedral basis and declines 40.3(2)° to the respective JT axis. The angle between atoms in the bridge Mn(2)−O(2A)−Mn(2)**, 97.38°, does not play role in the exchange. The distance Mn(2)−O(2A**) or (Mn(2**)−O(2A)) has no physical meaning of the bond length. The intrigue is that the empty $d_{x^2-y^2}$ orbital remains nearly orthogonal to this *p*-orbital of O(2A), so that a "ferromagnetic type" of hopping is forbidden.

We presume that strong displacement of Mn(2) (Mn(2**)) cation on the JT axis towards N(2F) (N(2F**)) may significantly change the symmetry of low laying energy levels so that the energies of $d_{x^2-y^2}$ and d_{z^2} orbitals become relatively close. Then the *p*-orbital of O(2A) inclining nearly 45° to the [O(2A),Mn(2),N(2F)] plane is able to mediate the ferromagnetic superexchange between d_{yz} of Mn(2) and d_{z^2} of Mn(2**) (and vice versa). For example, splitting of the spectroscopic terms of the high-spin *3d* Mn^{III} ion when lowering the symmetry from O_h to C_{2v} with the elongation axis perpendicular to the C_2 axis leads to the inversion of t_{2g} and e_g orbitals. So that the d_{yz} orbital has the highest energy and remains empty. The six-coordinated octahedral Mn^{III} ion has an orbitally degenerate ^5E_g ground electronic term that is split by the Jahn–Teller effect into $^5A_{1g}$ and $^5B_{1g}$ orbital singlet low-lying states. The $d_{x^2-y^2}$ and d_{z^2} orbitals are indeed mixed because

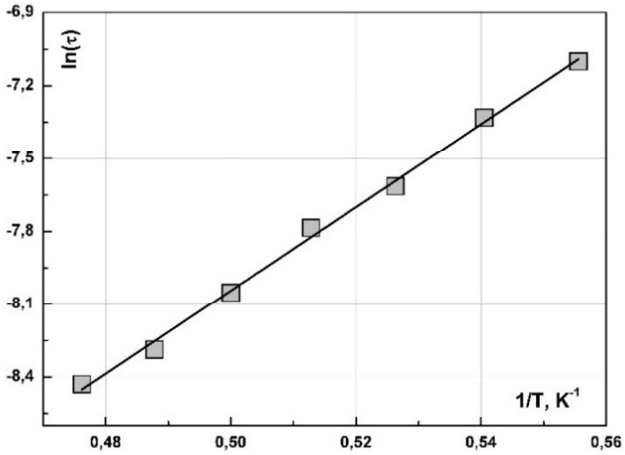

Fig. 9. Plot of relaxation time, ln(τ), vs temperature, 1/T, for a polycrystalline sample **3** determined from ac χ'' data. The solid line represents the Arrhenius fit with parameters: E_a=11.9 cm-1, τ_0=6.9·10-8 s (see text).

they show the same symmetry. Owing to the large mixing between the low-lying states, second-order spin-orbit coupling effects induce a large axial magnetic anisotropy, whose sign depends on the ground state, that is, on the nature of the axial tetragonal distortion.[17] For an axially elongated octahedral Mn^{III} environment, large negative D values are expected that can potentially lead to a large energy barrier for the magnetization reversal between the two lowest M_S=±2 states. In recent precise experiments on a mononuclear Mn^{III} complex $Ph_4P[Mn(opbaCl_2)(py)_2]$ ($H_4opbaCl_2$=*N,N'*-3,4-dichloro-*o*-phenylenebis(oxamic acid), py=pyridine, and Ph_4P^+= tetraphenylphosphonium cation) large single ion D value of −3.421(2) cm^{-1}, which is close to the result of current work, was confirmed.[17]

The above assumption in application to Mn^{III} complexes with saltmen^{2-} and naphtmen^{2-} ligands requires a detailed study of the symmetry of their low-lying *d*-states and second-order spin-orbit coupling effects.

Conclusions

To summarize, we have synthesized three new heterometallic Mn(III)-Fe(II) complexes containing the $[Mn^{III}(salpn)]^+$ and $[Fe(CN)_6]^{4-}$ fragments: $[\{Mn(salpn)(H_2O)\}_2\{Mn(salpn)(H_2O)_{0.7}(CH_3OH)_{0.3}\}_2Fe(CN)_6]\cdot n(H_2O/CH_3OH)$ (**2**), $[\{Mn(salpn)\}_4\{Mn(salpn)(H_2O)\}_2Fe(CN)_6]\{C(CN)_3\}_2\cdot 4H_2O$ (**3**) and $[\{Mn(salpn)(CH_3OH)_{0.67}(H_2O)_{0.33}\}_6Fe(CN)_6]\{ClO_4\}_2\cdot 8H_2O$ (**4**). The complexes **2**, **3** are products of the reaction between $[Mn(salpn)(H_2O)C(CN)_3]$ and $K_3[Fe(CN)_6]$ and **4** forms in the reaction of $[Mn_2(salpn)_2(H_2O)_2](ClO_4)_2$ with $(NH_4)_4[Fe(CN)_6]$. Interestingly, that the tricyanometanide ligand reduces Fe(III) to Fe(II). **3** has also been obtained in the reaction of $[Mn(salpn)(H_2O)C(CN)_3]$ with ferrocyanide. The complexes **2** and **4** comprise discrete pentanuclear $[Mn^{III}_4Fe^{II}]$ and heptanuclear $[Mn^{III}_6Fe^{II}]$ units, respectively. In contrast, the heptanuclear $[Mn^{III}_6Fe^{II}]$ units in **3** are linked into one-dimensional polymeric chains by double phenolate bridges $[\{Mn(NC)(salpn)\}(\mu\text{–}O_{phenolate})_2\{Mn(NC)(salpn)\}]$ between the Mn(2) and Mn(2**) centers (Fig. 2, 3). The Mn^{III}–Mn^{III} distance in the dimer is 3.491(1). The Jahn–Teller elongation axes in the Mn(2) and Mn(2**) octahedrons lie along the axial directions with Mn−$N_{cyanide}$ and Mn−$O_{phenolate}$ bonds of 2.167(3) and 2.697(2) Å. Ferromagnetic coupling is found in the Mn^{III} dimers. The exchange coupling constant $J_{22'}$ = 0.64 cm^{-1} and zero-field splitting parameter D= −3.4±0.5 cm^{-1} are determined by numerical simulations of the magnetic susceptibility data within the Heisenberg−Van Vleck model. The magnetization data at 2.0 K also speaks in favor of large axial magnetic anisotropy in the dimer moments. The *ac*- susceptibility data indicate slow-relaxation processes obeying Arrhenius lay with the activation energy E_a= 11.89 cm^{-1} (17.1 K). The enhancement of single ion anisotropy of Mn^{III} spin moment is explained in terms of specific distortions caused and stabilized by π-stacking of the salpn ligands. By lowering symmetry, the distortions may mix the low-lying *d*-states promoting the ferromagnetic coupling. Numerical simulation of the partial spin contributions to the total magnetic susceptibility confirms the infinite chains ferromagnetically coupled dimers in **3.**

Experimental

Materials

All chemicals and solvents used in synthesis were reagent grade and were used without further purification. The precursors, $[Mn_2(salpn)_2(H_2O)_2](ClO_4)_2$ and $[Mn(salpn)C(CN)_3(H_2O)]$, were prepared according to the literature procedures.[3f, 6]

Caution: Cyanides are highly toxic and should be handled with great caution. We worked at the mmol scale and all the preparations were performed in a well ventilated hood.

Preparations

$[\{Mn(salpn)\}_4\{Mn(salpn)(H_2O)\}_2Fe(CN)_6]\{C(CN)_3\}_2 4H_2O$ (3). A solution of $(NH_4)_4[Fe(CN)_6]$ (8.33 mg, 0.029 mmol) in 5 ml of water was added to a solution of $[Mn(salpn)C(CN)_3(H_2O)]$ (78 mg, 0.174 mmol) in 10 ml of methanol. The mixture was heated to 50 ˚C. After stirring for 30 min, the resulting dark brown solution was filtered. The filtrate was left undisturbed at room temperature for one week to produce dark brown single crystals suitable for X-ray analysis. The crystals were collected by suction filtration, washed with water, and air-dried. Yield: 65% based on $[Mn(salpn)C(CN)_3(H_2O)]$. Anal. found: C, 54.84; H, 4.38; N, 13.35%. Calcd for $C_{116}H_{108}FeMn_6N_{24}O_{18}$: C, 55.46; H, 4.30; N, 13.39%. Characteristic IR data (cm^{-1}): $\nu_{C\equiv N}$: 2159 (tricyanometanide-ion), $\nu_{C\equiv N}$: 2050 (bridge); $\nu_{C=N}$: 1613 (imine).

$[\{Mn(salpn)(CH_3OH)_{0.67}(H_2O)_{0.33}\}_6Fe(CN)_6]\{ClO_4\}_2 8H_2O$ (4). The procedure was the same as for **3** except that $[Mn(salpn)C(CN)_3(H_2O)]$ was replaced by $[Mn_2(salpn)_2(H_2O)_2](ClO_4)_2$ (3 eq., 0.087 mmol). Yield: 42% based on $[Mn_2(salpn)_2(H_2O)_2](ClO_4)_2$. Anal. found: C, 49.18; H, 4.69; N, 9.43%. Calcd for $C_{112}H_{132}Cl_2FeMn_6N_{18}O_{34}$: C, 49.25; H, 4.84; N, 9.23%. Characteristic IR data (cm^{-1}): $\nu_{C\equiv N}$: 2048 (bridge); $\nu_{C=N}$: 1611 (imine); $\nu_{Cl\text{-}O}$: 1084 (ClO_4).

Physical measurements

Elemental analyses for C, H and N were performed on a vario MICRO cube analyzing device. The IR spectra were recorded in the range of 500-4000 cm^{-1} using Varian 3100 FTIR Excalibur Series spectrophotometer.

Variable-temperature magnetic susceptibility measurement of **3** was performed with a Quantum Design MPMS SQUID magnetometer.

X-ray single crystal diffraction data were collected at different temperatures on an Oxford Diffraction Gemini-R diffractometer (for **2** and **4**) and on a Bruker SMART APEX II diffractometer (for **3**) using MoK_α radiation [λ(MoK_α) = 0.71073 Å, graphite monochromator, ω-scans]. Single crystals of **2-4** were taken from the mother liquid using nylon loop with paratone oil and immediately transferred into cold nitrogen stream of the diffractometer. Data reduction with empirical absorption correction of experimental intensities was made with the CrysAlisPro software[18] and Bruker SAINT Plus program package.[19]

The structures were solved by direct methods and refined by a full-matrix lest squares method using SHELX97 program.[20] Non-hydrogen atoms were refined anysotropically except for oxygen atoms of free water molecules. Hydrogen atoms were placed in the idealized positions. The hydrogen atoms of coordinated water molecules and part of free water molecules were found from difference Fourier maps. Hydrogen atoms of other non-coordinated water molecules and disordered water ligands were not localized but included into the composition of **2-4**. Main crystal data and the X-ray data collection and refinement statistics for **2-4** are listed in Table 4. Additional structure refinement details for **2** are given in Supporting Information.

Acknowledgments

This work was supported by the RFBR grant 13-03-12418 and Presidium of the Russian Academy of Sciences, project No. 12M-23-2054, grant for support of the leading scientific schools No. 1540.2014.2. We thank P.Yu. Barzilovich and K.A. Lyssenko for an X-ray experiment on a Bruker APEX II diffractometer. Y.N.Sh thanks Alex Mogilner and UC Davis for providing the visiting scholar position and computational resources.

Table 4. Crystal data and structural refinement parameters for the complexes **2**-**4**

	2	**3**	**4**
Chemical formula	$C_{74.6}H_{69.8}FeMn_4N_{14}O_{13.6}$	$C_{116}H_{108}FeMn_6N_{24}O_{18}$	$C_{112}H_{132}Cl_2FeMn_6N_{18}O_{34}$
Formula weight	1662.31	2511.75	2730.75
Cell setting	monoclinic	monoclinic	cubic
Space group, Z	$P2_1/c$, 2	$P2_1/n$, 2	$Pa\bar{3}$, 4
Temperature (K)	150(2)	100(2)	120(2)
a (Å)	19.644(4)	13.392(4)	22.9655(4)
b (Å)	14.872(2)	17.417(6)	22.9655(4)
c (Å)	14.938(2)	24.344(7)	22.9655(4)
α (°)	90	90	90
β (°)	110.31(2)	102.555(7)	90
γ (°)	90	90	90
Cell volume (Å^3)	4093(1)	5542(3)	12112.3(4)
ρ (Mg/m^3)	1.349	1.505	1.497
μ, cm^{-1}	8.40	8.68	8.52
Refls collected/unique	26171 / 11460	51647 / 14691	58343 / 6117
R_{int}	0.0645	0.0951	0.0384
θ_{max} (°)	31.14	29.00	31.16
Parameters refined	732	754	267
Final R_1, wR_2 [I>2σ(I)]	0.0722, 0.1455	0.0491, 0.1020	0.0394, 0.1044
Goodness-of-fit	1.004	1.011	1.008

Notes and references

[a] *Institute of problems of Chemical Physics, Chernogolovka, Moscow District, Academician Semenov av. 1, 142432 Russian Federation. E-mail: , slavaoven@mail.ru; yagubski@icp.ac.ru Fax: +7 496-5225636; Tel: +7 495-9935707*

[b] *Institute of Solid State Physics, Chernogolovka, Moscow District, Academician Ossipyan str. 2, 142432 Russian Federation. E-mail: zorina@issp.ac.ru; Fax: +7 496-5228160; Tel: +7 496-5221982*

[c] *Institute of Metal Physics, S .Kovalevskaya St. 18, 620990 Ekaterinburg, Russian Federation. Fax: +7 343-3745244; Tel: +7 343-3740230*

[d] *Department of Mathematics, University of California, Davis, CA 95616, USA. E-mail: yshvachko@ucdavis.edu; Fax: +7 343-3745244; Tel: +7 343-3740230*

† Electronic Supplementary Information (ESI) available: Fig S1-S6. CCDC reference numbers 986574 (**2**), 986575 (**3**) and 986576 (**4**). These data can be obtained free of charge from The Cambridge Crystallographic Data Centre via www.ccdc.cam.ac.uk/data_request/cif. For ESI and crystallographic data in CIF or other electronic format see DOI: 10.1039/b000000x/

1 (*a*) F.M. Ashmawy, C.A. McAuliffe, R.V. (Dick) Parish and J. Tames, *J. Chem. Soc. Dalton Trans*, 1985, 1391; (*b*) A.R. Oki and D.J. Hodgson, *Inorg. Chim. Acta.*, 1990, **179**, 65; (*c*) H. Miyasaka, N. Matsumoto, H. Okawa, N. Re, E. Gallo and C. Floriani, *Angew. Chem.,Int. Ed. Eng.*, 1995, **34**, 1446; (*d*) N. Re, E. Gallo,C. Floriani, H. Miyasaka and N. Matsumoto, *Inorg. Chem.*, 1996, **35**, 6004; (*e*) F. Sakamoto, T. Sumiya, M. Fujita, T. Tada, X-S. Tan, E. Suzuki, I. Okura and Y. Fujii, *Chem. Lett.*, 1998, **27**, 1127; (*f*) H. Miyasaka, R. Clérac, T. Ishii, H. Chang, S. Kitagawa and M. Yamashita, *J. Chem. Soc. Dalton Trans.*, 2002, 1528.

2 (*a*) Y. Cringh, S.W. Gordon-Wylie, R.E. Norman, G.R. Clark, S.T. Weintraub and C.P. Horwitz, *Inorg. Chem.*, 1997, *36*, 4968; (*b*) Ch.E. Hulme, M. Watkinson, M. Haynes, C. A. McAuliffe, N. Jaiboon, B. Beagley, A. Sousa, M.R. Bermejo and M. Fondo, *J. Chem. Soc. Dalton Trans.*, 1997, 1805; (*c*) N. Matsumoto, Z.L. Zhong, H. Okawa and S. Kida, *Inorg. Chim. Acta*, 1989, **160**, 153; (*d*) A. Garcia-Deibe, A. Sousa, M.R. Bermejo, P.P. MacRory, C. A. McAuliffe, R.G.Pritchard and M. Hellowel, *Chem. Commun.*, 1991, 728; (*e*) M.R. Bermejo, A. Castineiras, J.C. Garcia-Monteagudo, M. Rey, A. Sousa, M. Watkinson, C.A. McAuliffe, R.G. Pritchard and R.L. Beddoes, *J. Chem. Soc. Dalton Trans.*, 1996, 2935; (*f*) M. Mikuriya, Y. Yamato and T. Tokii, *Bull. Chem. Soc. Jpn.*, 1992, **65**, 1466; (*g*) H. Li, Z.J. Zhong, C. Duan, X. You, T.C.W. Mak and B. Wu, *J. Coord. Chem.*, 1997, **41**, 183; (*h*) B.J. Kennedy and K. Murray, *Inorg. Chem.*, 1985, **24**, 1552.

3 (*a*) H. Miyasaka, N. Matsumoto, H. Okawa, N. Re, E. Gallo and C. Floriani, *J. Am. Chem. Soc.*, 1996, **118**, 981; (*b*) Y. Sato, H. Miyasaka, N. Matsumoto and H. Okawa, *Inorg. Chem. Acta*, 1996, **247**, 57; (*c*) H.-L. Shyu, Ho-H. Wie and Yu. Wang, *Inorg. Chim.*

Acta., 1999, **290**, 8; (*d*) N. Matsumoto, H. Okawa, S. Kida, T. Ogawa and A. Ohyoshi, *Bull. Chem. Soc. Jpn.*, 1989, **62**, 3812; (*e*) H. Miyasaka, R. Clérac, W. Wernsdorfer, L. Lecren, C. Bonhomme, K.-I. Sugiura and M. Yamashita, *Angew. Chem,. Int. Ed. Eng.*, 2004, **43**, 2801; (*f*) L. Lecren, W. Wernsdorfer, Y.-G. Li, A. Vindigni, H. Miyasaka and R. Clérac, *J. Am. Chem. Soc.*, 2007, **129**, 5045; (*g*) Z. Lu, M. Yuan, F. Pan, S. Gao, D. Zhang and D. Zhu, *Inorg. Chem.*, 2006, 45, 3538.

4 (*a*) H.J. Choi, J.J. Sokol and J.R. Long, *Inorg. Chem.*, 2004, **43**, 1606; (*b*) H. Miyasaka, H.Ieda, N. Matsumoto, N. Re, R. Crescenzi and R. Floriani, *Inorg. Chem.*, 1998, **38**, 255; (*c*) H.H. Ko, J.H. Lim, H.S. Yoo, J.S. Kang, H.C. Kim, E.K. Koh and C.S. Hong, *Dalton Trans.*, 2007, 2070; (*d*) P. Przychodzen, M. Rams, C. Guyard-Duhayon, B. Sieklucka, *Inorg. Chem. Commun.*, 2005, **8**, 350; (*e*) M. Ferbinteanu, H. Miyasaki, W. Wernsdorfer, K. Nakata, K. Sugiura, M. Yamashita, C. Coulon and R. Clérac, *J. Am. Chem. Soc.*, 2005, **127**, 3090; (*f*) H.S. Yoo, H.H. Ko, D.W. Ryo, J.W Lee, J.H. Yoon, W.R. Lee, H.C. Kim, E.K. Kon and C.S. Hong, *Inorg. Chem.*, 2009, **48**, 5617; (*g*) H. Miyasaka, H. Okawa, A. Miyazaki and T. Enoki, *Inorg. Chem.*, 1998, **37**, 4878; (*h*) H.Z. Kou, Z.H. Ni, B.C. Zhou and R.J. Wang, *Inorg. Chem. Commun.*, 2004, **7**, 1150; (*i*) H.-B. Zhou, J. Wang, H.-S. Wang, Y.-L. Xu, X.-J. Song, Y. Song and X.-Z. You. *Inorg. Chem.*, 2011, **50**, 6868; (j) J. Dreiser, K.S. Pedersen, A. Schnegg, K. Holldack, J. Nehrkorn, M. Sigrist, P. Tregenna-Piggott, H. Mutka, H. Weihe, V.S. Mironov, J. Bendix and O. Waldmann, *Chem. Eur. J.*, 2013, **19**, 3693; (*k*) H. Miyasaka, A. Saitoh and S. Abe, *Coord. Chem. Rev.*, 2007, **251**, 2622; (*l*) H. Miyasaka, T. Madanbashi, A. Saitoh, N. Motokawa, R. Ishikawa, M. Yamashita, S. Bahr, W. Wernsdorfer and R. Clérac, *Chem. Eur. J.*, 2012, **18**, 3942; (*m*) J.N. Rebilly and T.Mallah, *in Single-Molecule Magnets and Related Phenomena*, ed. R. Winpenny, 2006, 103; (*n*) K. Pedersen, J. Bendix and R. Clérac, *Chem. Comm.*, 2014, **50**, 4396, and references therein.

5 (*a*) H. Miyasaka and R. Clérac, *Bull. Chem. Soc. Jpn.*, 2005, 78, 1725; (*b*) R. Clerac, H. Miyasaka, M. Yamashita and C. Coulon, *J. Am. Chem. Soc.*, 2002, **124**, 12837; (*c*) H. Miyasaka, T. Madanbashi, K. Sugimoto, Y. Nakazawa, Y. Wernsdorfer, K. Sugiura, M. Yamashita, C. Coulon and R. Clérac, *Chem. Eur. J.*, 2006, **12**, 7028; (*d*) H. Sun, Z. Wang and S. Gao, *Coord. Chem. Rev.*, 2010, **254**, 1081; (*e*) W.-X. Zhang, R. Ishikawa, B. Breedlove and M. Yamashita, *RSC Advances*, 2013, **3**, 3772.

6 V.A. Kopotkov, S.V. Simonov, O.V. Koplak, A.I. Dmitriev, E.B. Yagubskii, *Russ. Chem. Bull., Int. Ed.,* 2013, **62**, 1777.

7 (*a*) R.J. Parker,. D.C.R. Hockless, B. Moubaraki, K.S. Murray and L. Spiccia, *Chem. Commun.*, 1996, 2789; (*b*) F.Thetiot, S. Triki, and J.S. Pala, *New J. Chem.*, 2002, **26**, 2002; (*c*) R.J. Parker, L. Spiccia, B. Moubaraki, K.S. Murray, D.C.R. Hockless, A.D. Rae, and A.C. Willis, *Inorg. Chem*., 2002, **41**, 2489; (*d*) C.S. Hong, Y.S. You, *Inorg. Chim. Acta*, 2004, **357**, 3271.

8 S-F. Si, J-K. Tang, Z-Q Liu, D-Z Liao, Z-H. Jiang, S-P Yan and P. Cheng, *Inorg. Chem. Commun.*, 2003, **6**, 1109.

9 P. Przychodzen, K. Lewinski, M. Balanda, R. Pelka, M. Rams, T. Wasiutynski, C. Guyard-Duhayon and B. Sieklucka., *Inorg. Chem.*, 2004, **43**, 2967.

10 R. Ababei, Y.-G. Li, O. Roubeau, M. Kalisz, N. Bréfuel, C. Coulon, E. Harté, X. Liu, C. Mathonière and R. Clérac, *New J. Chem.*, 2009, **33**, 1237.

11 (*a*) X. Shen, B. Li, J. Zou, H. Hu and Z. Xu, *J. Mol. Struct.*, 2003, 325; (*b*) D. Zhang, H. Wang, Y. Chen, Z.-H. Ni, L. Tian and J. Jiang, *Inorg. Chem.*, 2009, **48**, 11215.

12 J.-J. Zhang and A. Lachgar, *J. Am. Chem. Soc.*, 2007, **129**, 250.

13 C. Yang, Q.-L. Wang, J. Qi, Y. Ma, S.-P. Yan, G.-M. Yang, P. Cheng and D.-Z. Liao, *Inorg. Chem.*, 2011, **50**, 4006.

14 (*a*) J.-J. Zhang, H.-J. Zhou and A. Lachgar, *Angew. Chem. Int. Ed.*, 2007, **46**, 4995; (*b*) J.-J. Zhang, C.S. Day and A. Lachgar, *CrystEngComm*, 2011, **13**, 133.

15 E. Bill, *julX 1.4.1 Simulation of molecular magnetic data software*, Max-Planck Institut for Bioinorganic Chemistry, Mülheim/Ruhr, May 2008; Matrix diagonalization is realized with the routine 'zheev' from the LAPACK numerical package

16 (*a*) J. B. Goodenough, *Magnetism and the Chemical Bond*, Interscience, New York, 1963; (b) D. I. Khomskii, *Basic Aspects of the Quantum Theory of Solids: Order and Elementary Excitations*, Cambridge University Press, New York, 2010.

17 J. Vallejo, A. Pascual-Alvarez, J. Cano, I. Castro, M. Julve, F. Lloret, J. Krzystek, G. De Munno, D. Armentano, W. Wernsdorfer, R. Ruiz-Garcia, and E. Pardo, *Angew. Chem. Int. Ed.*, 2013, **52**, 14075.

18 *CrysAlisPro, Version 1.171.33*, Oxford Diffraction Ltd., Oxford, UK, 2010.

19 *Bruker (2001) SAINT-Plus*, Bruker AXS Inc., Madison, Wisconsin, USA.

20 G. M. Sheldrick, *Acta Cryst., Sect. A*, 2008, **64**, 112.

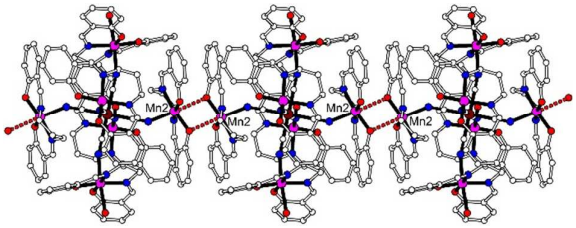

The tricyanomethanide-ligand reduces Fe(III) to Fe(II) yielding the discrete $[\{Mn(salpn)(H_2O)\}_2\{Mn(salpn)(H_2O)_{0.7}(CH_3OH)_{0.3}\}_2Fe(CN)_6]\cdot n(H_2O/CH_3OH)$ and chain $[\{Mn(salpn)\}_4\{Mn(salpn)(H_2O)\}_2Fe(CN)_6]\{C(CN)_3\}_2\cdot 4H_2O$ complexes.